Nationaal Lucht- en Ruimtevaartlaboratorium
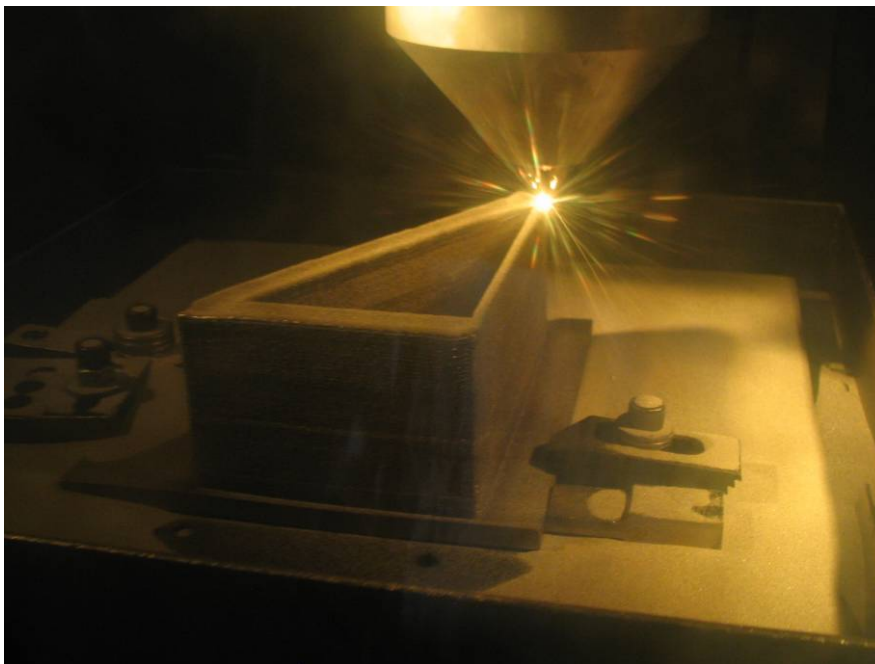
National Aerospace Laboratory NLR

Executive summary

Evaluation of the microstructure and mechanical properties of laser additive manufactured gas turbine alloys Ti-6Al-4V and Inconel 718

Problem area

Laser Additive Manufacturing (LAM) is a technique where a high-power laser is focused on a metal substrate to create a localized melt pool. Metal powder is injected into the melt pool, where it solidifies as the part is rastered back and forth according to a 3D CAD pattern. LAM is an innovative process that can reduce manufacturing lead time, costs and raw materials consumption for gas turbine parts. In addition, it can improve the functionality of these components.

However, LAM requires very high quality standards when used for gas turbine components to fulfil the aerospace safety regulations.

Description of work

The objective of this program was to get an impression of the technique and to demonstrate the capabilities of the LAM process for creating new and spare parts which are viable for Dutch industry.

Two 'components' were manufactured by Optomec using the

This report is based on a presentation held at the RTO AVT-163 Specialists' meeting, Bonn, 19-21 October 2009.

Evaluation of the microstructure and mechanical properties of laser additive manufactured gas turbine alloys Ti-6Al-4V and Inconel 718

LAM (LENS™) technique; one from Inconel 718 and the other from Ti-6Al-4V. The components were made with standard process parameters. The components were given a standard heat treatment prior to the cut-up for machining the test samples.

The tensile properties are measured with test samples cut from the laser track and built up directions. High cycle fatigue (HCF) tests were performed on both alloys to create a stress vs. cycles curve. Fracture surfaces were examined from both alloys. Crack initiations and their relation to porosity and the microstructures have been reviewed. The results for Ti-6Al-4V are compared with results from LAM literature to assess the current LAM capabilities. Since literature on LAM-fabricated Inconel 718 is scarce, the results for Inconel 718 are compared with wrought IN718 and, owing to the same component geometry and process conditions, to the LAM-fabricated Ti-6Al-4V.

Results and conclusions
Both components contained many macro and micro defects, such as large cavities, lack of bonding between layers and porosity. The yield stress and ultimate tensile strength of both materials are similar to wrought material, however due to the defects the elongation to failure is lower and shows large scatter. For the limited data set of Ti-6Al-4V, the fatigue performance is better than wrought material. However, the presence of large pores decreases the performance significantly, making the fatigue performance similar to wrought Ti-6Al-4V. For the limited data set of Inconel 718, the fatigue performance is similar to wrought material, even though the material contains many small pores. Lack of bonding between layers decreases the fatigue performance of Inconel 718 accordingly.

Applicability
The laser powder deposition technique demonstrated to be capable of producing the same material properties as wrought material for component shaped geometries with both, thick and thin walls. However, further development work and process parameter optimization should be done to decrease the number of defects and increase the reliability and reproducibility.

NLR-TP-2009-656

Evaluation of the microstructure and mechanical properties of laser additive manufactured gas turbine alloys Ti-6Al-4V and Inconel 718
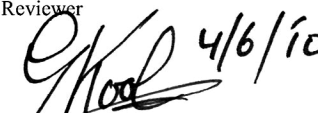
E. Amsterdam
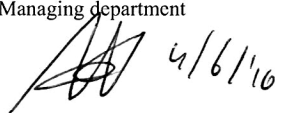
Customer	Netherlands Agency for Aerospace Programmes (NIVR)
Contract number	59710N
Owner	National Aerospace Laboratory NLR
Division NLR	Aerospace Vehicles
Distribution	Unlimited
Classification of title	Unclassified
	May 2010

Approved by:

Author	Reviewer	Managing department
04-06 '10	4/6/10	4/6/'10

Summary

In hostile battleground environments, like Afghanistan, there is a high need to reconstruct or repair worn integrated engine parts to keep the aircraft flying. For critical engine parts the mechanical properties of the repaired part should be comparable as the original part. Laser additive manufacturing (LAM) is one of the techniques that can be used in the field, because it can create high quality components of any given shape from feedstock powders. The objective of this program was to get an impression of the technique and to demonstrate the capabilities of the LAM process for creating new and spare parts which are viable for Dutch industry. To evaluate the current status of the LAM technology, two identical components have been fabricated at Optomec by the LAM (LENS™) technique. One component was made of Ti-6Al-4V and the other of Inconel 718, both widely used gas turbine engine materials. The components have been made with standard process parameters. The components were given a standard heat treatment prior to the cut-up for machining the test samples. Test samples were cut from the laser track and build directions to examine the tensile properties for both orientations. High cycle fatigue (HCF) tests were performed on round samples to create a stress vs. cycles curve for both alloys. The fracture surfaces of the tensile and HCF samples were examined for both alloys, with special attention to crack initiation and its relation to the microstructure. For a good assessment of the current LAM technology status the results for Ti-6Al-4V are compared with results from LAM-literature. Since literature on LAM fabricated Inconel 718 is scarce, the results for Inconel 718 are compared with wrought IN718 and, owing to the same component geometry and process conditions, to the LAM fabricated Ti-6Al-4V.

Contents

Abbreviations

BD	Build Direction
CAD	Computer Aided Design
LD	Longitudinal Direction
BLISK	BLaded dISK
HCF	High Cycle Fatigue
LAM	Laser Additive Manufacturing
LENS	Laser Engineered Net Shaping
NIVR	Netherlands Agency for Aerospace Programmes (NIVR)
NLR	National Aerospace Laboratory NLR
RO	Run Out
SEM	Scanning Electron Microscope
EDX	Energy Dispersive analysis of X-rays
UTS	Ultimate Tensile Strength

1 Introduction

The use of integrated parts, like blade integrated disks (BLISKs), in military gas turbine engines is increasing due to higher engine performance demands and the objective to reduce the number of engine parts. In hostile battleground environments, like Afghanistan, there is a high need to reconstruct or repair worn integrated engine parts to keep the aircraft flying. For critical engine parts the mechanical properties of the repaired part should be comparable as the original part. LAM is one of the techniques that can be used in the field, because it can create high quality components of any given shape from feedstock powders [1]. The objective of this program was to get an impression of the LAM technique and to demonstrate the capabilities of the LAM process for creating new and spare parts which are viable for Dutch industry. For an assessment of the current LAM technology status, two identical components have been fabricated by the laser engineered net shaping (LENS) technique. One component was made of Ti-6Al-4V and the other of Inconel 718. The shape of the components is chosen such that it incorporates a thin wall, a thick wall and different angles at which the walls meet (see Fig. 1). Microstructure, tensile and fatigue samples were cut from the components to assess the microstructure and the mechanical properties.

2 Experimental set-up

Two identical components have been fabricated by the LENS™ technique at Optomec in Albuquerque (NM), USA. One component was made of Ti-6Al-4V and the other one of Inconel 718 (see Fig. 1). The components were made with standard process parameters. After receiving the components, they were given a standard heat treatment; for Ti-6Al-4V this is a solution heat treatment at 970°C for 1hr, water quench and age at 538°C for 4hr, air cool [2]. For Inconel 718, a post weld heat treatment was selected; 1093°C for 1 hour, cool to 718°C with 84°C per hour, 718°C for 4 hours, cool at 56°C per hour to 620°C, 620°C for 16 hours, cool at 139°C per hour to below 371°C, air cool [3].

Round fatigue samples have been cut from wall A (see Fig. 1) and were polished to a roughness Ra< 0.2 μm. The fatigue samples have been tested at different stress levels on an electro-magnetic resonance machine Amsler HFP 422 with a frequency of 110 and 140 Hz for the Ti-6Al-4V and Inconel 718 samples respectively. The frequency depends on the material stiffness. The length of the samples is oriented parallel to the build direction (BD).

Flat tensile samples were cut from the thin wall B and round tensile samples were cut from wall C, according to ASTM E8 testing standard. The length of the samples is oriented parallel (BD) and perpendicular (LD) to the build direction. The gage length of the flat and round tensile samples is 32 mm and 36 mm, respectively. Instron test machines, with a 100 kN and 300 kN loadcell, were used for the flat and round samples respectively. The tests have been performed at room temperature and the displacement speed of the crosshead was 1 mm/min (quasistatic). An MTS clip gage with a gauge length of 25 mm was used to measure the strain.

Microstructure samples have been cut from the top of the thick wall, the middle of the thin wall and at the root of the build (both the thick and the thin wall, including the substrate). For each location, cross-sections were made parallel (half way the thickness) and perpendicular to the wall. Optical- and scanning electron microscopy (SEM) have been used to characterise the microstructure. The SEM, equipped with energy dispersive analysis of X-rays (EDX), was used to determine the chemical composition. The porosity was measured by optical microscopy and the macrohardness by an Instron 930 testor using a 5 kg load. Both measurements have been performed before etching. Ti-6Al-4V was etched with Keller's reagent and Inconel 718 with Beraha II to reveal the microstructures.

3 Results

3.1 Components

After a visual inspection of the Ti-6Al-4V component, the following can be remarked (see Fig. 1a): the 7 mm thick substrate is warped. The surface of the component is shiny and rough. The thickness of all the walls is 2.5 mm larger than specified. Due to the curved substrate the height is less than specified. There are some defects present in the component that results from droplets of liquid metal that fall from the powder nozzle onto the build. This is encircled in black on the component, see Fig. 1a.

After a visual inspection of the Inconel 718 component, the following can be remarked (see Fig 1b): the 7 mm thick substrate is also warped. The surface of the component is rough (large droplets are attached to the walls) and the thickness of all the walls is 1.1-1.5 mm larger than specified. Due to the curved substrate the height is less than specified. At the top of wall C, the wall no longer has the thickness of the root. Large grooves are present from partially melting of the wall. This probably occurred because the system was not equipped with a melt pool detector.

3.2 Microstructure

The chemical composition of both components is measured at several locations. The results are given in Table 1. None of the alloying elements are less than specified; for Inconel 718 some elements are even slightly higher than specified.

The grain structure of the thin wall is given in Figure 2. The grains are smaller near the interface with the substrate and the grain size increases with the build-up height. This is typical for laser beam deposited material [4]. The grains extend across multiple tracks in the horizontal and vertical (build-up) direction. Some pores are present at the interface with the substrate. The microstructure of the Ti-6Al-4V component consists of a Widmanstätten structure and represents a normal casting structure.

The microstructure of the Inconel 718 component consists also of a grain structure with small grains at the root of the build-up. The grain size increases for increasing build-up height. The long axis of large extended grains ranges from 100 to 250 microns and the short axis of the same grains from 50-100 microns. Carbides are present in the microstructure (white areas, see Fig. 3a), as well as micro-porosity (see also black dots in Fig. 3a). Small white needles can be observed, which are γ'' precipitates. Larger white needles can be observed on the grain boundary, which are δ (delta) precipitates. The meta-stable γ'' phase can transform into the δ (delta) precipitate, which has the same chemical composition but a different crystal structure and morphology. After etching, the γ/γ' distribution was made visible; cuboids and spheroids can be distinguished. The cuboid size is about 600 nanometer.

Figure 4 shows a cross-section of the thin wall at the half height of the component. A light and a dark area can be distinguished and the difference is caused by a difference in etching. The difference in etching is caused by the difference in δ-phase density. Why the density of the δ-phase is higher at the upper half of the component is unknown, but it can be related to the excessive heat input.

The porosity was determined with optical microscopy for the cross-sections and is given in Table 2. The porosity of the Ti-6Al-4V cross-sections seems to increase towards the root of the build-up for the thin and thick wall (see also Fig. 2a). The Inconel 718 samples contain many pores with a wide range of diameters. Figure 3a shows that very small pores, with a size < 1 μm, are present. The measurement of the porosity, with diameters more than 4 μm, has been done by image analysis on optical microscope images. For Inconel 718 the porosity seems to increase towards the top of the component and a clear difference can be observed between the areas with

and without the δ-phase. The relative density of the Inconel 718 component is 99.7% and is lower than that of the Ti-6Al-4V component, which has a relative density of 99.97%.

3.3 Tensile properties

Ti-6Al-4V. Table 3 shows the tensile properties of the round and flat Ti-6Al-4V samples. For both, the round and the flat samples, there is one sample (Ti-C6 and Ti-B2) that failed under a low stress due to insufficient bonding between the build-up layers. For sample Ti-C6, very large cavities (1-2 mm) and lack of bonding are present (see Fig. 5). The other round tensile samples all have similar tensile properties in terms of yield stress, ultimate tensile strength (UTS) and elongation to failure. The flat samples show a higher yield stress and UTS, but with a large range of elongations to failure. No effect of the orientation of the samples can be observed. The fracture surfaces of the samples Ti-C1 to Ti-C5 and Ti-B1, Ti-B3 to Ti-B10 show features of ductile failure.

The Vickers macrohardness (HV5kg) of wall B (thin wall) and C (thick wall) is HV 390 ± 2 and HV 363 ± 6 respectively, corresponding to the flat and round tensile samples. Herewith the hardness measurements confirm that the strength of the material in wall B is 7.5% larger than that of wall C.

Inconel 718. Table 4 shows the tensile properties of the round and flat Inconel 718 samples. From the six round samples, three failed outside the gauge length and the fracture surfaces showed the absence of bonding between the layers for several tracks, see Fig. 5 (and are therefore not included in Table 4). Sample IN-C4 failed within the gauge length, but the fracture surfaces also show an area of lack of bonding between the layers. Sample IN-C5 failed outside the gauge length, but did not show signs of lack of bonding. For the flat samples, five of the eleven samples showed strange behaviour and are not included in Table 4. These samples failed, at low elongations, near the radius and exhibited a lower Young's modulus. For the remaining flat samples there is a large scatter in the elongation to failure. For samples with an elongation to failure < 10%, the UTS increases with increasing yield stress.

The fracture surfaces, of the flat Inconel 718 samples with a low elongation to failure, are rather flat and perpendicular to the load direction. For the samples with a higher elongation to failure, the fracture surface looks more jagged and is slanted with respect to the loading direction. All samples that are removed from the upper part of the component, where the δ-phases are observed, showed the strange behaviour mentioned above and have a low elongation to failure. The fracture surfaces of these sample show failure of the brittle δ-phase (see Fig. 6). All fracture surfaces of the round and flat samples showed numerous pores with different sizes.

3.4 Fatigue

Figure 7 shows the S-N curves of Ti-6Al-4V and Inconel 718. Figure 7a contains fewer points, because some samples with a diameter of 4.5 mm failed in the thread. Therefore the diameter of the remaining samples is reduced to 4 mm. The sample tested at 800 MPa has a diameter of 4.5 mm and the other samples have a diameter of 4.0 mm. Two samples of each material were stopped at $5 \cdot 10^7$ cycles and were tested again (indicated by the squares). One of the Ti-6Al-4V samples that was stopped at $5 \cdot 10^7$ cycles, fractured in the thread when tested at a higher stress.

3.5 Fatigue fracture surfaces

The fatigue fracture surfaces of the Ti-6Al-4V samples show crack initiation from pores. The sample tested at 800 MPa showed nucleation from a large round pore (see Fig. 8). For the sample tested at 700 MPa (with the lowest number of cycles), the crack initiated in a pore just beneath the surface. For the run out (RO) sample, tested again at 700 MPa, the crack initiated from a very small interdendritic shrinkage pore exactly on the centreline of the test sample. In the low ΔK region around the initiation point, flat cleavage-like facets of the α-phase can be observed (see Fig. 8). The size of the cleavage like facets corresponds with the size of the Widmanstätten structure (see Figs. 2 and 5).

The fatigue fracture surfaces of the Inconel 718 samples show crack initiation from the surface. Near the initiation point, the fracture surface is facetted. The majority of the area of the fracture surfaces is caused by overload and much porosity was observed on these areas for all the samples. None of the samples fractured in the thread and therefore Inconel 718 is not as notch sensitive as Ti-6Al-4V. From literature it is known that notch behaviour is a concern for Ti-6Al-4V [2]. The fracture surface of the sample tested at 800 MPa showed tracks of lack of bonding between layers.

4   Discussion

The yield stress and UTS values of the Ti-6Al-4V samples are similar to literature values for solution heat treated and aged material (yield stress = 1103 MPa, UTS = 1172) [2]. Both the yield stress and the UTS of the flat Ti-6Al-4V samples are larger than that of the round samples and the range of elongation to failure values is lower. Also the hardness of the material in wall B (thin) is larger (7.5%) than that of wall A (thick). This indicates that there is an intrinsic difference in strength between the two. This can originate from a difference in the microstructure, either created during the build-up with the laser due to potentially different wall temperatures or during the heat treatment from a possible difference in cooling rates. The Ti-

6Al-4V component is water quenched during the heat treatment and therefore there are differences in cooling rates for the thin and thick walls.

The yield stress and UTS of the Inconel 718 samples are also similar to the literature values for solution heat treated and aged material (yield stress = 1131 MPa, UTS = 1331) [3]. The high cooling rates are not present in the heat treatment of Inconel 718 and the difference in strength between the flat and round samples is also not observed. Since the fatigue samples are cut from a thick wall (A) the yield stress and the UTS are equal to that of the round tensile samples (also indicated by the hardness measurements). However, there is a very large difference in the elongation to failure compared with literature (23% [3]). To a large extent, this is due to macro defects such as lack of bonding between the layers (for the elongation to failure ≤2.4%). The sample with an elongation to failure >2.4% did not show signs of macro defects, but showed many pores. Even the fracture surfaces of the flat and round samples with an elongation to failure ≥14.2% showed many pores.

The fatigue performance of Ti-6Al-4V is better compared with literature data on wrought annealed samples with a similar yield (925 MPa) and tensile strength (1000 MPa) [2]. However, when large pores, or subsurface pores, are present the fatigue performance is similar to wrought annealed samples. The reference data points in Fig. 7a correspond to samples of Ti-6Al-4V produced by the same technique and producer [5]. Since Ti-6Al-4V is notch sensitive, the presence of a pore decreases the number of cycles to failure significantly (see Fig. 7a).

Although there are a limited number of data points for Inconel 718, the following can be said: in spite of the many small pores, the fatigue performance of the Inconel 718 samples is similar to annealed and aged sheet material [3]. The presence of macro defects does have a detrimental effect on the fatigue performance, as can be seen for the 800 MPa sample.

5 Conclusion

Two identical components of Ti-6Al-4V and Inconel 718 are fabricated by Optomec using the LENS™ technique. Both components contained many macro and micro defects, such as large cavities, lack of bonding between layers and porosity. The yield stress and ultimate tensile strength of both materials are similar to wrought material, however due to the defects the elongation to failure is lower and shows large scatter. For the limited data set of Ti-6Al-4V, the fatigue performance is better than wrought material. However, the presence of large pores decreases the performance significantly, making the fatigue performance similar to wrought Ti-

11

6Al-4V. For the limited data set of Inconel 718, the fatigue performance is similar to wrought material, even though the material contains many small pores. Lack of bonding between layers decreases the fatigue performance of Inconel 718 accordingly.

The laser powder deposition technique demonstrated to be capable of producing the same material properties as wrought material for component shaped geometries with both, thick and thin walls. However, further development work and process parameter optimization should be done to decrease the number of defects and increase the reliability and reproducibility.

Acknowledgement

References

[1] Hedges, M. and Calder, N. (2006), Meeting Proceedings RTO-MP-AVT-139, Paper 13, Neuilly-sur-Seine, France

[2] Donachie, M.J. (2000). *Titanium – A Technical Guide (2nd Ed.)*, ASM int., Ohio.

[3] Aerospace Structural Metals Handbook, 1997 ed. (1997), Purdue University, West Lafayette.

[4] Oliveira, U.O.B de (2007), *Laser treatment of alloys: processing, microstructure and structural properties*, Doctoral thesis, University of Groningen, Groningen.

[5] Grylls, R. (2006) LENS process white paper: fatigue testing of LENS Ti-6-4, Optomec internal report,
www.optomec.com/downloads/EADS_Fatigue_Testing_Technical_Brief_2006.pdf

Table 1 Chemical composition (wt%) of the components and the nominal composition of Ti-6Al-4V and Inconel 718 [3]

(a) Ti-6Al-4V

	Ti	Al	V
Measured (avg. + st. dev. of 5 measurements)	90.2 ± 0.2	5.9 ± 0.1	3.9 ± 0.1
Nominal composition	Balance	Min. 5.50 Max. 6.75	Min. 3.50 Max. 4.50

(b) Inconel 718

		Ni	Cr	Nb	Mo	Ti	Al	Fe
Measured (avg. + st. dev.of 5 meas.)		50.5 ± 0.4	19.9 ± 0.2	5.7 ± 0.2	3.4 ± 0.2	1.11 ± 0.05	0.71 ± 0.05	18.6 ± 0.2
Nominal composition	Min.	50	17	4.75	2.80	0.65	0.20	Balance
	Max.	55	21	5.50	3.30	1.15	0.80	

Table 2 Porosity of (a) the Ti-6Al-4V and (b) the Inconel 718 component

(a) Ti-6Al-4V

Section (wall, location, plane)	Section size (mm²)	Largest pore (μm)	Number of pores			
			>2 μm	25-50 μm	50-100 μm	larger than 100 μm
Thick, top, parallel	208	32	2	1	-	-
Thick, top, perp.	224	25	6	1	-	-
Thin, middle, parallel	196	25	1	1	-	-
Thin, middle, perp.	29	-	-	-	-	-
Thick, bottom, parallel	95	70	6	4	3	-
Thick, bottom, perp.	64	86	8	3	3	-
Thin, bottom, parallel	19	56	2	2	1	-
Thin, bottom, perp.	99	16	3	-	-	-

The largest diameter is given as the size of the pore.

(b) Inconel 718

Section (wall, location, plane)	Section size (mm²)	Largest pore (μm)	Pore density (pore/mm2)			
			>2 μm	25-50 μm	50-100 μm	larger than 100 μm
Thick, top, parallel (δ-phase)	22.1	112	11.4	1.0	0.2	0.05
Thick, top, perp. (δ-phase)	22.1	62	10.0	0.9	0.2	-
Thin, middle, parallel dark section (δ-phase)	22.1	69	6.7	1.2	0.2	-
Thin, middle, parallel light section	22.1	36	7.1	0.3	-	-
Thin, bottom, perp.	12.5	111	4.3	0.3	0.08	0.08
Thick, bottom, perp.	24.3	62	9.1	0.4	0.04	-

The largest diameter is given as the size of the pore.

Note: the number of pores is given in (a) and the pore density in (b).

15

Table 3 Tensile properties of (a) round and (b) flat Ti-6Al-4V samples. The samples are ordered from the lowest to the highest elongation to failure. The length of the samples is oriented parallel (BD) and perpendicular (LD) to the build direction.

(a) Round samples

Sample	Orientation	Yield stress (MPa)	UTS (MPa)	Elongation to failure (%)
Ti-C6	LD		191	0.3
Ti-C4	LD	989	1089	9.2
Ti-C1	BD	943	1073	9.8
Ti-C5	LD	957	1057	10.9
Ti-C2	BD	935	1073	11.1
Ti-C3	BD	947	1051	13.3

(b) Flat samples

Sample	Orientation	Yield stress (MPa)	UTS (MPa)	Elongation to failure (%)
Ti-B2	BD		263	0.2
Ti-B5	LD	1025	1138	3.4
Ti-B9	LD	1076	1162	3.4
Ti-B8	LD	1085	1168	3.7
Ti-B4	LD	1014	1162	4.0
Ti-B6	LD	1063	1135	6.6
Ti-B7	LD	1065	1162	7.8
Ti-B10	LD	1034	1145	7.9
Ti-B3	BD	1062	1151	8.4
Ti-B1	BD	1028	1130	10.0

16

Table 4 Tensile properties of (a) round and (b) flat Inconel 718 samples

(a) Round samples

Sample	Orientation	Yield stress (MPa)	UTS (MPa)	Elongation to failure (%)
IN-C4	LD	661	966	2.4
IN-C5	LD	998	1322	-
IN-C6	LD	1014	1350	18.4

(b) Flat samples

Sample	Orientation	Yield stress (MPa)	UTS (MPa)	Elongation to failure (%)
IN-B5	LD	635	958	2.6
IN-B7	LD	1002	1271	5.5
IN-B8	LD	1049	1296	6.5
IN-B10	LD	1057	1362	-
IN-B11	LD	1107	1415	14.2
IN-B9	LD	1060	1369	15.3

For the samples IN-C5 and -B10, the elongation to failure is missing, since the sample failed outside the extensiometer area.
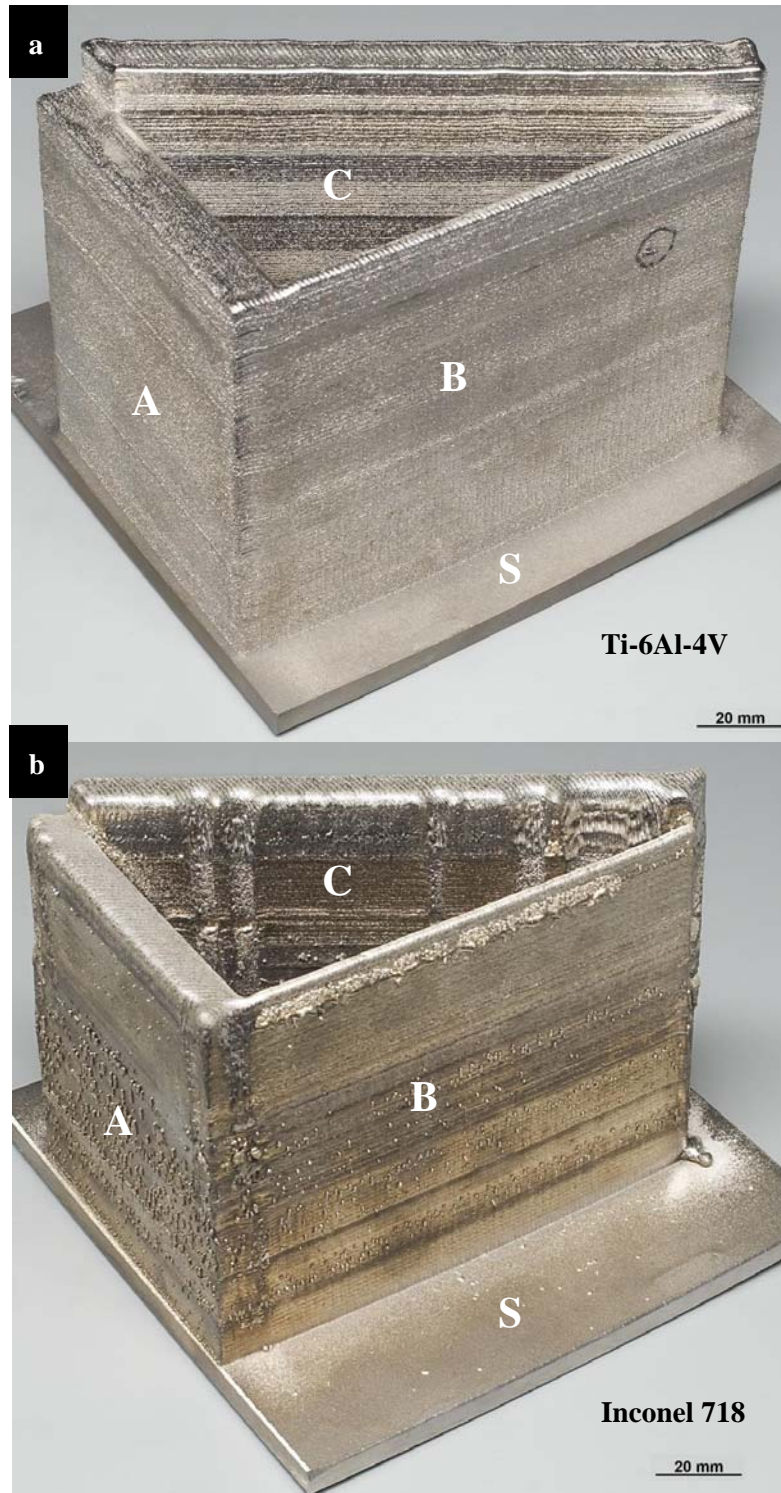
Figure 1 Photographs of the (a) Ti-6Al-4V and (b) Inconel 718 component fabricated with laser powder deposition. The letters indicate wall A, B, C and the substrate (S). The black circle on the Ti-6Al-4V sample indicates a building defect.

18
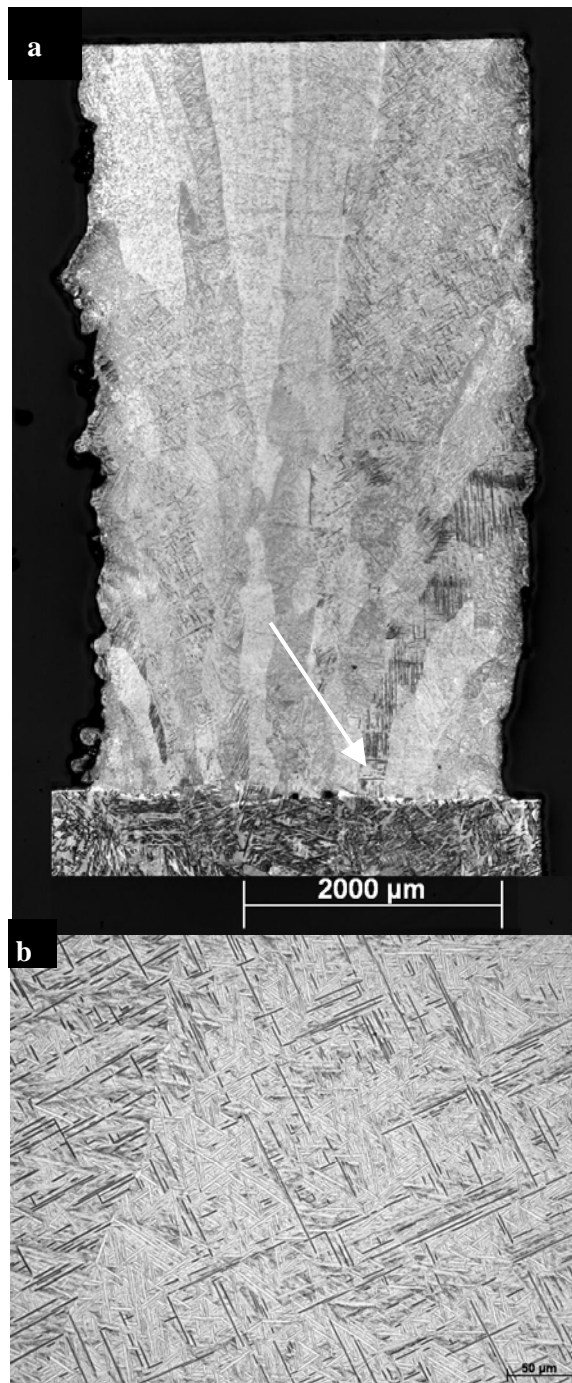
Figure 2 (a) Grain structure of thin wall and the substrate of the Ti-6Al-4V component. Some pores can be seen on the boundary with the substrate (indicated by the white arrow). (b) Widmanstätten microstructure of the Ti-6Al-4V component.
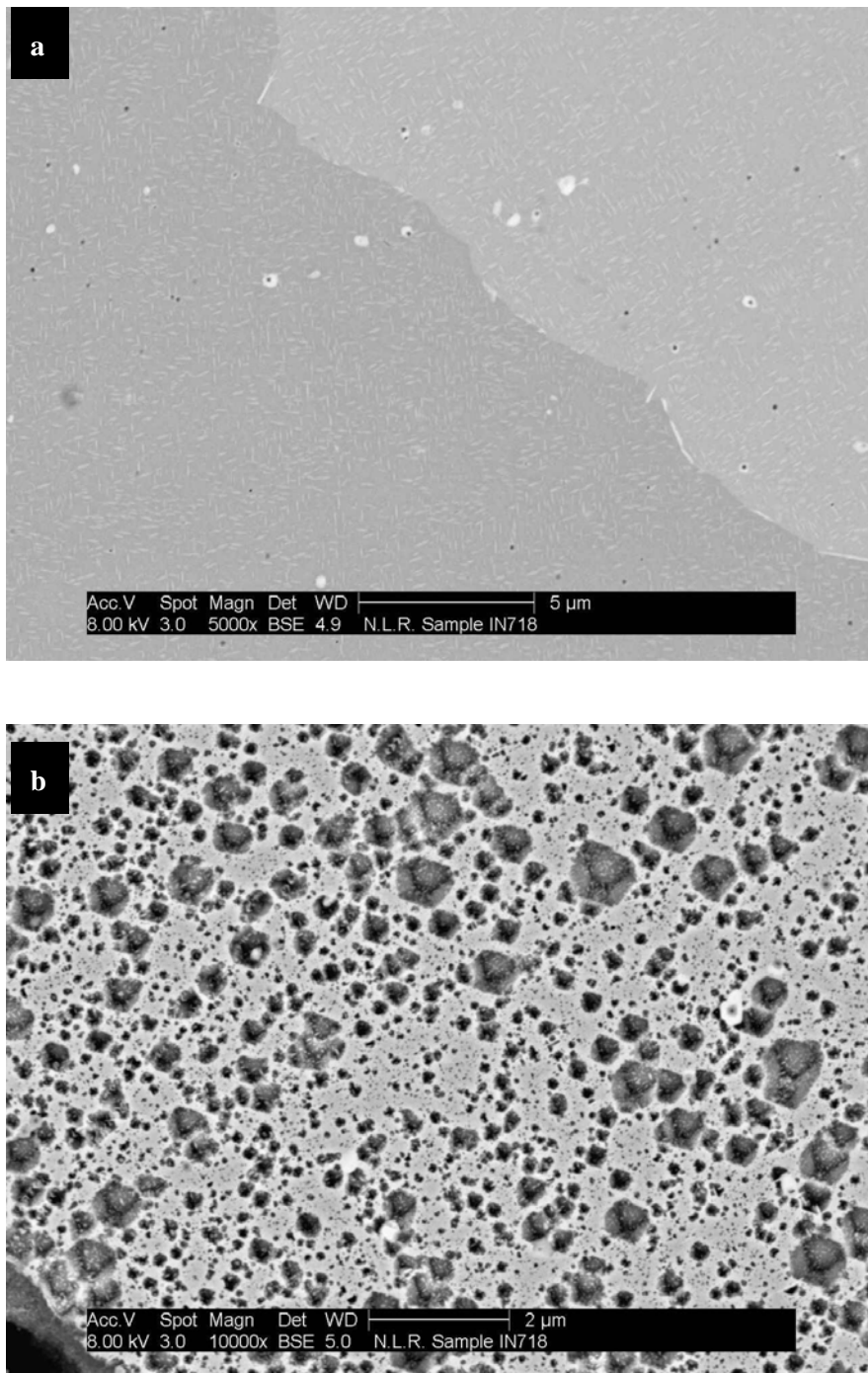
Figure 3 Microstructure of the Inconel 718 component; (a) before etching, showing different grains, carbides (white), γ´´ (small white needles), δ-phases (larger white needles on the grain boundary) and porosity (black dots), (b) after etching showing the γ/γ´ distribution. Cuboids and spheroids can be observed.
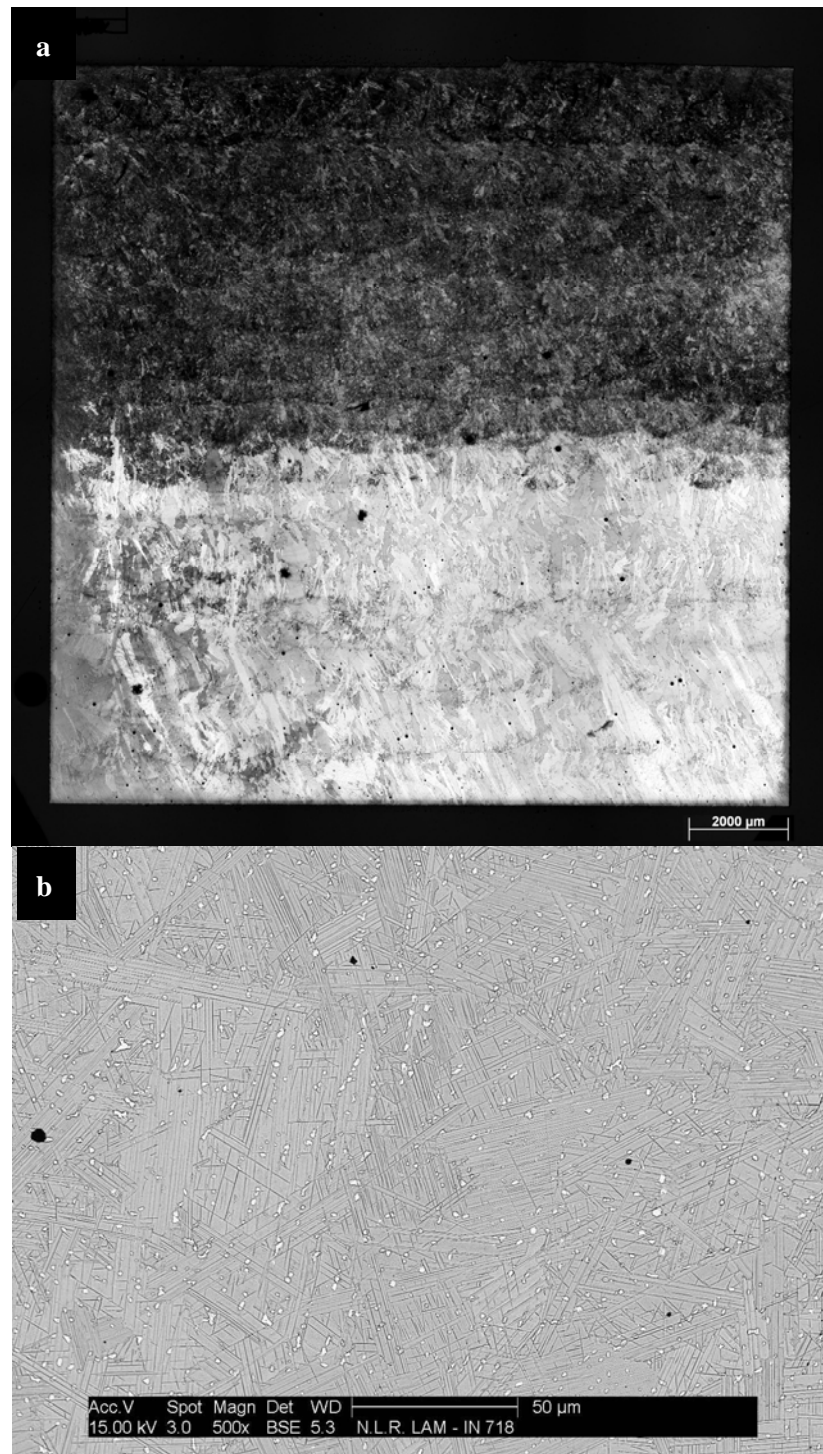
Figure 4 (a) Longitudinal cross-section of the thin wall from half way the height of the component. A light and a dark area can be distinguished and the difference is caused by a difference in etching. (b) Microstructure of the upper half part of the build of the Inconel 718 component. The microstructure contains a lot of δ-phases.
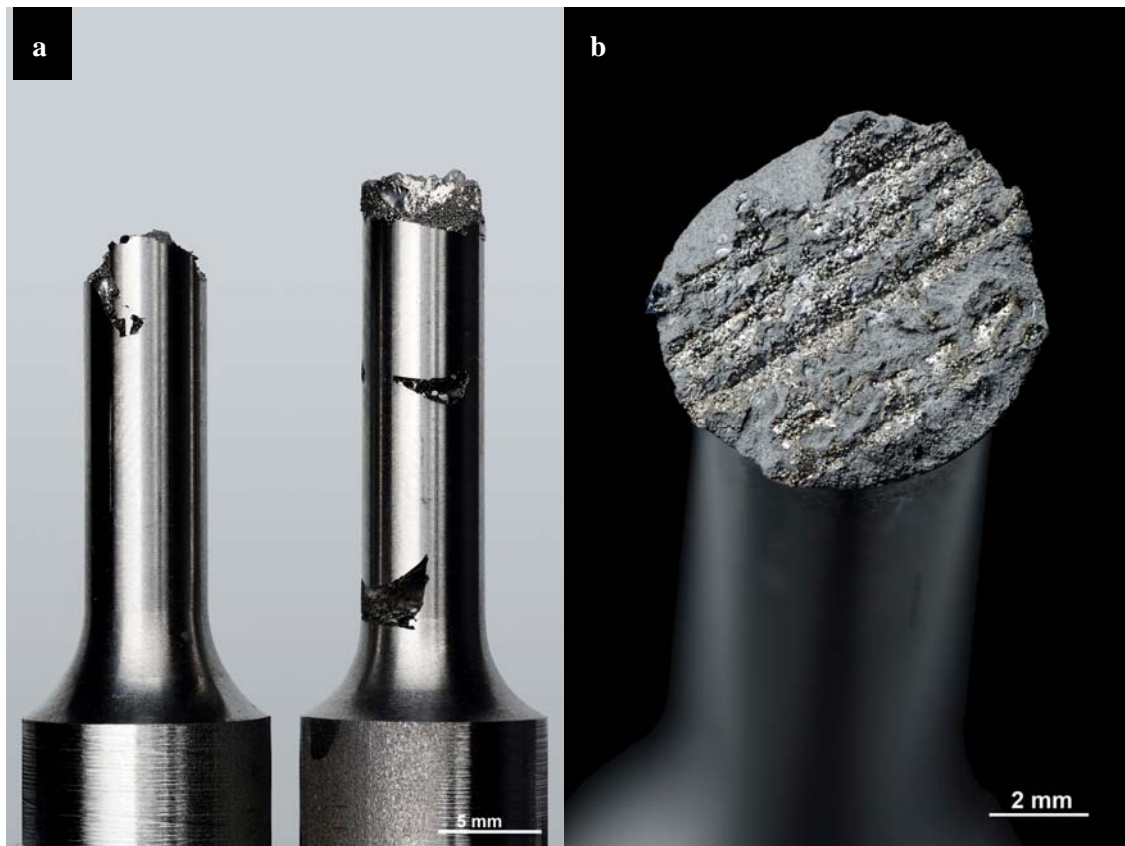
Figure 5 (a) Appearance of a round Ti-6Al-4V sample, multiple defects are present in the sample. The sample fractured at a large defect. (b) Fracture surface of a round Inconel 718 sample. The fracture surface show tracks of lack of bonding.
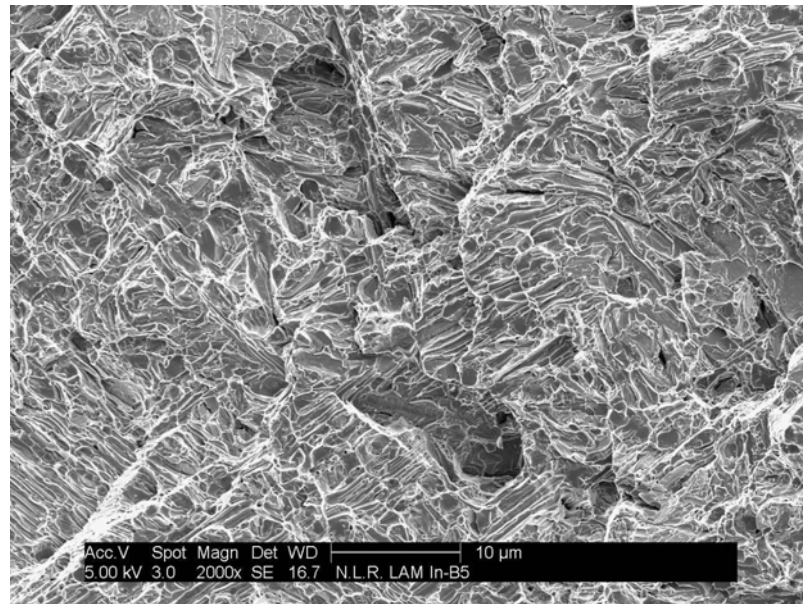
Figure 6 Fracture surface of a flat Inconel IN-B5 sample. The fracture surface shows fractured
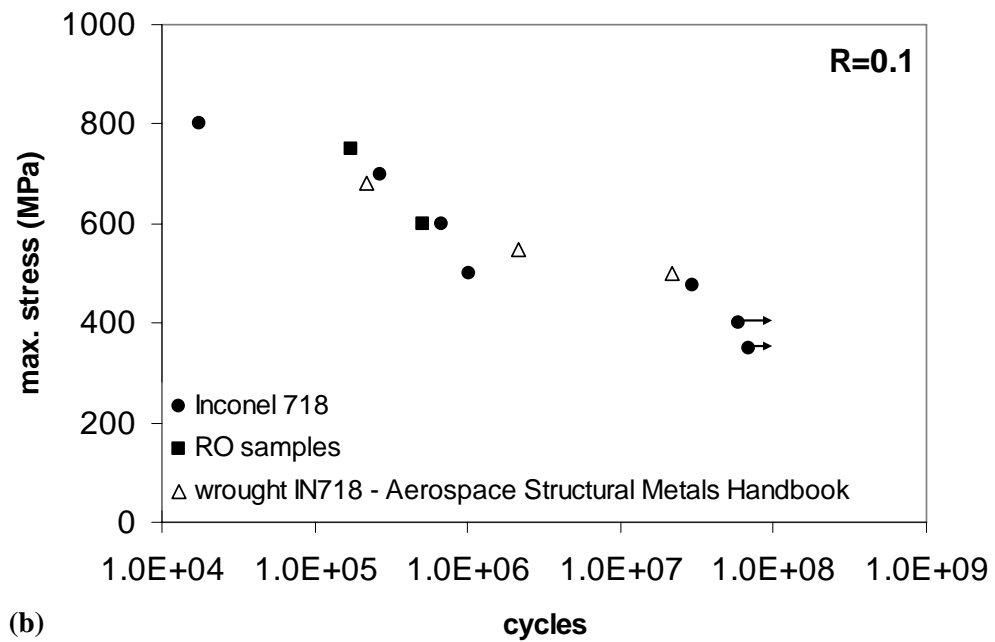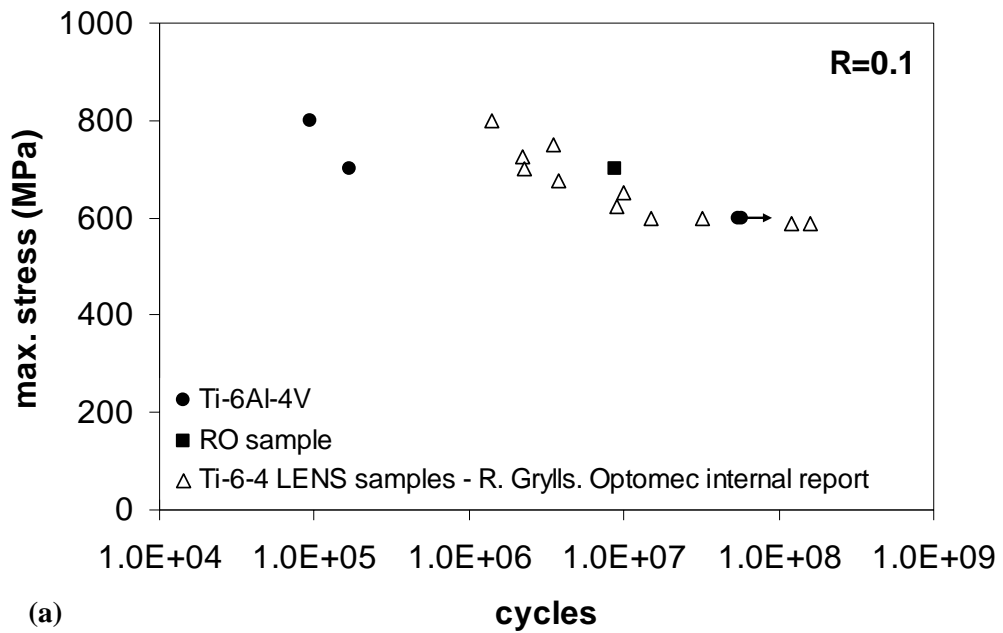needles markings.

Figure 7 S-N curve of the (a) Ti-6Al-4V and (b) Inconel 718 samples fabricated with the LENS technique. Two samples of each material were stopped at 5·10^7 cycles (indicated by the arrows) and tested again at a higher stress level (run out (RO) samples, indicated by the squares). Orientation of the samples is in the build-up direction.
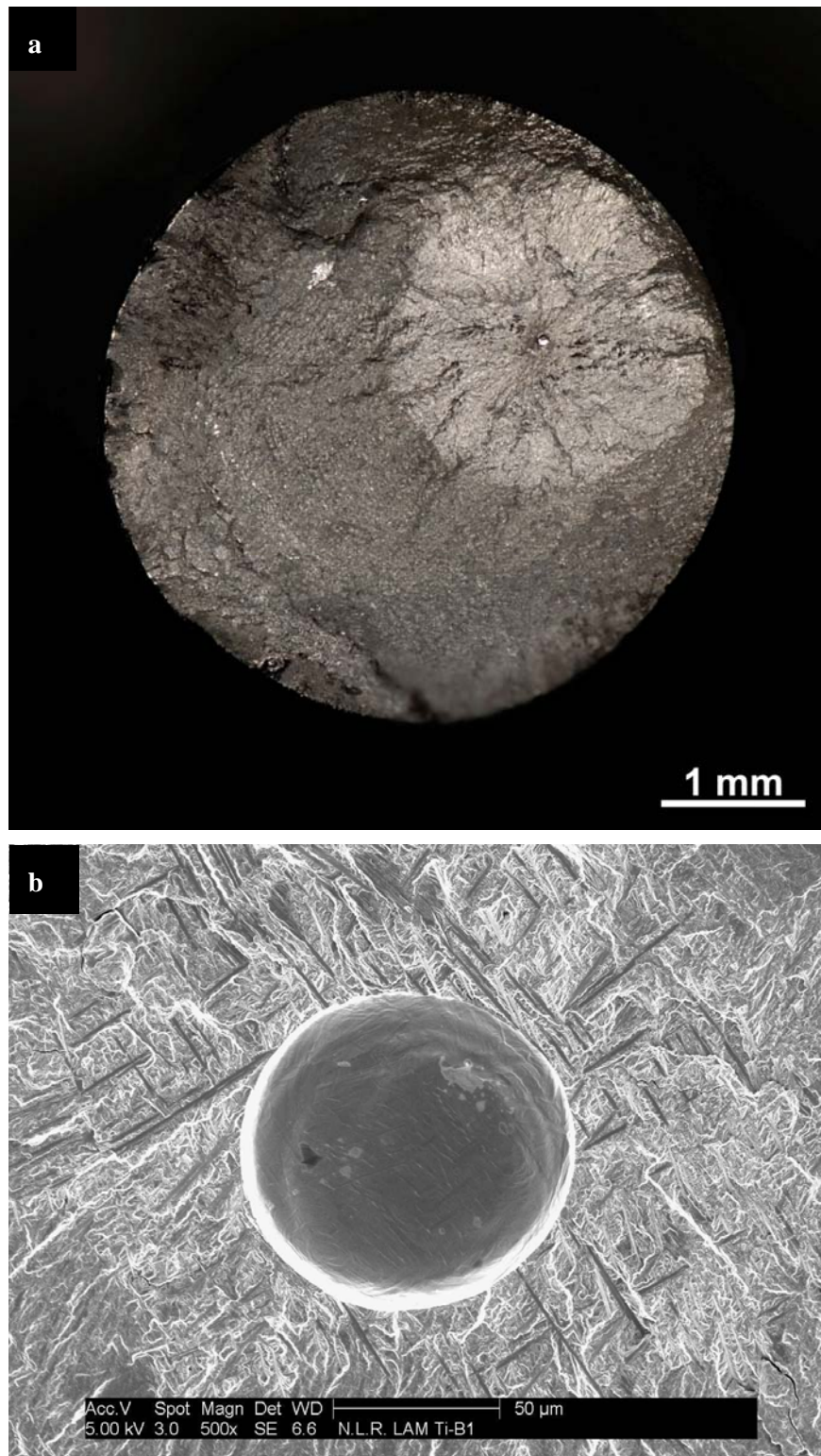
Figure 8 (a) Fracture surface of the Ti-6Al-4V HCF sample that is tested at 800 MPa. A circular crack initiated and grew from a pore with a diameter of 102 µm. (b) SEM image of the pore in (a). In the low ∆K region around the initiation point, flat cleavage-like facets of the α-phase can be observed.